Journal of Hydrology 598 (2021) 126438

Contents lists available at ScienceDirect

Journal of Hydrology

journal homepage: www.elsevier.com/locate/jhydrol

Research papers

Increasing LSPIV performances by exploiting the seeding distribution index at different spatial scales

Silvano Fortunato Dal Sasso [a,*], Alonso Pizarro [b], Sophie Pearce [c], Ian Maddock [c], Salvatore Manfreda [b]

[a] Department of European and Mediterranean Cultures: Architecture, Environment and Cultural Heritage (DICEM), University of Basilicata, 75100 Matera, Italy
[b] Department of Civil, Architectural and Environmental Engineering, University of Naples Federico II, 80125 Naples, Italy
[c] School of Science and the Environment, University of Worcester, Worcester, UK

ARTICLE INFO

This manuscript was handled by Corrado Corradini, Editor-in-Chief, with the assistance of Valentina Ciriello, Associate Editor

Keywords:
Image velocimetry
UAS
River flow monitoring
LSPIV
Seeding metrics
Seeding Distribution Index
Frame footage

ABSTRACT

Image-based approaches for surface velocity estimations are becoming increasingly popular because of the increasing need for low-cost river flow monitoring methods. In this context, seeding characteristics and dynamics along the video footage represent one of the key variables influencing image velocimetry results. Recent studies highlight the need to identify parameter settings based on local flow conditions and environmental factors apriori, making the use of image velocimetry approaches hard to automatise for continuous monitoring. The seeding distribution index (SDI) – recently introduced by the authors – identifies the best frame window length of a video to analyse, reducing the computational loads and improving image velocimetry performance. In this work, we propose a method based on an average SDI time series threshold with noise filtering. This method was tested on three case studies in Italy and validated on one in the UK, where a relatively high number of measurements was available. Following this method, we observed an error reduction of 20–39% with respect to the analysis of the full video. This beneficial effect appears even more evident when the optimisation is applied at sub-sector scales, in cases where the SDI shows a marked variability along the cross-section. Finally, an empirical parameter τ was proposed, calibrated, and validated for practical uses to define the SDI threshold. τ showed relatively stable values in the different contexts where it has been applied. Application of the seeding index to image-based velocimetry for surface flow velocity estimates is likely to enhance measurement accuracy in future studies.

1. Introduction

Technological developments, the advent of Unmanned Aerial Systems (UASs), open-source software and smartphone applications – and the increasing need of feasible measurements are promoting the use of image velocimetry techniques for streamflow observations (Manfreda et al., 2018; Eltner et al., 2020). Optical methods allow the estimation of surface velocity in rivers by analysing surface images captured from the banks or above the water surface. The measurement of surface velocity, especially during floods, is a more practical way to derive river flows combining depth-averaged water velocities and cross-sectional area information. The main advantages of using these non-contact technologies concern reducing risk, the low cost of operations, and the possibility of application at inaccessible locations during extreme hydrological events (Le Coz et al., 2010; Le Boursicaud et al., 2016). Different image velocimetry techniques have been proposed in recent years that use optical images of the stream water surface to derive surface velocity 2D maps (Pearce et al., 2020). These methods include the classical correlation-based algorithms such as Large Scale Particle Image Velocimetry (LSPIV - Fujita et al., 1998) and Large Scale Particle Tracking Velocimetry (LSPTV - Brevis et al., 2011), but also new approaches of optical flow based on the detection of patterns of image intensity, such as Space-Time Image Velocimetry (STIV - Fujita et al., 2007), Surface Structure Image Velocimetry (SSIV - Leitão et al., 2018), Optical Tracking Velocimetry (OTV - Tauro et al., 2020) and Kanade–Lucas Tomasi Image Velocimetry (KLT-IV – Perks, 2020). All these methods have been successfully applied on images acquired from both fixed and mobile platforms (UAS) allowing the reconstruction of instantaneous flow velocity fields and the estimation of surface velocity in rivers with errors less than 20% (Kim et al., 2008; Le Coz et al., 2010; Detert et al.,

* Corresponding author.
E-mail address: silvano.dalsasso@unibas.it (S.F. Dal Sasso).

https://doi.org/10.1016/j.jhydrol.2021.126438
Received 8 February 2021; Received in revised form 15 April 2021; Accepted 5 May 2021
Available online 8 May 2021

2017; Kinzel and Legleiter, 2019; Eltner et al., 2020).

Similarly, recent advancements in topographic surveys with modern portable GPS, laser profilers, radar systems, and Structure-from-Motion (SfM) photogrammetry has enabled the acquisition of bathymetry and water depth in a more efficient way (Kinzel and Legleiter, 2019; Manfreda et al., 2019a). Remarkably, stream flows can be optically estimated as well when river bathymetry and a vertical velocity profile are known. In this direction, Bandini et al. (2020) recently explored the novel idea to estimate river discharge using both the Manning equation and mid-section method equation relying on bathymetry knowledge, surface velocity measurements from UAS, and water surface slope calculation.

However, although these approaches are rapidly increasing, the errors and uncertainty in the use of these methods persist. On the one hand, image velocimetry techniques employ parameters and settings that require a detailed level of expertise (e.g., interrogation area size, cross-correlation parameters). These parameters are related to the specific field conditions – such as seeding density, tracers' dimension, frame rate, flow velocity itself – and are not easily identifiable. Pearce et al. (2020) performed a sensitivity analysis to identify the best setting configuration for different optical techniques. Rozos et al., (2020) suggested a statistical approach to overcome the subjectivity of the selection of the parameter settings exploring the impact of parameter uncertainty on the results of the image velocimetry methods. On the other hand, the efficiency of these methods can be influenced by environmental factors (e.g., wind, light reflection and shadows), local hydraulic conditions (e.g., flow regime, flow velocity and directions), and operational practises (e.g., seeding deployment, camera movements) (Muste et al., 2008; Kim et al., 2008; Tauro et al., 2017). We have recently shown that the dynamics on time of seeding characteristics showed statistical significance on image-based performances (Dal Sasso et al., 2020). With respect to seeding conditions, the image velocimetry application by detecting and matching natural features (turbulence ripples, differences in colour due to suspended sediments and natural debris) still remains a challenge. Generally, the deployment of artificial tracers is necessary to improve these methods' accuracy (Detert et al., 2017).

Moreover, the number of frames to analyse is still an issue. A systematic reduction of errors is observed in numerical experiments (Manfreda et al., 2019b) and laboratory flumes (Samarage et al. 2012) by increasing the number of frames. This evidence is due to the fact that a higher number of frames increases the number of velocity samples in space and can help to smooths out outliers and noise with a consequent reduction of errors (Pizarro et al., 2020a and Pizarro et al., 2020b). This effect is particularly evident for low seeding conditions and where particles are not uniformly distributed over the entire frame sequences. However, this beneficial effect is not always observed in natural environments, where considering a large number of frames leads to increasing the occurrences of possible environmental disturbances over the video sequence (e.g., camera movements, environmental noise). For instance, Strelnikova et al. (2020) observed that a significant increase in the number of processed image pairs might negatively influence ensemble correlation results, significantly increasing the computational costs. Pizarro et al. (2020b), in their field experiments, showed that the use of a long frame sequence has no significant influence for improving final results. Moreover, intense computational times and hardware sources are needed to analyse and store long video time series. The processing time increases as a function of the number of frames, the extension of the Region of Interest (ROI), and the number of features detected (Perks, 2020). For this reason, generally, a reference sequence of frames in which tracers are visible is arbitrarily selected and extracted for image velocimetry processing.

In this regard, Pizarro et al. (2020a) and Pizarro et al. (2020b) recently introduced the Seeding Distribution Index (SDI) as a parameter that synthesises the seeding conditions in the field, merging seeding and spatial distribution characteristics. This dimensionless index was formulated using numerical experiments and tested in some field case studies for describing the heterogeneous spatial distribution of tracers and the tendency to form clusters. The evidence shows that this index can be a good descriptor for identifying the portion of the video with the best seeding condition and consequently, can be useful to improve image velocimetry performance.

Considering these issues and these recent findings, there is an overall need to harmonise these techniques for the scientific community, technicians, and practitioners to obtain more accurate surface flow velocity estimations. For this purpose, Perks et al. (2020a) collected different field experiences placed in six countries in which streamflow measurements were performed using fixed or mobile cameras (mounted on drones) coupled with image velocimetry techniques. This was a successful trial to test setting parameters, new algorithms, and establish practical guidelines of surface velocimetry estimations form optical cameras.

Applying the outcomes of these recent studies, this work investigates a possible strategy for minimising the errors in surface velocity estimations identifying the best frame window based on the characteristics of seeding in space and time. For this purpose, this work explored the possibility of applying image velocimetry techniques at the scale of the entire cross-section (sector) and at the local scale (sub-sectors) to improve the quality of the optical estimations. Moreover, a unique empirical parameter, calibrated on three case studies and validated on a further, was derived. It can represent a comprehensive reference to calculate SDI threshold with only a knowledge of seeding density and independently from field experiments' specific characteristics.

2. Field case studies and image data

In this work, three different case studies were analysed to identify a unique empirical SDI threshold and isolate the best frame footage for optimising image-based surface velocity estimates. The calibration dataset includes measurements performed on three field case studies at the Brenta, Noce, and Bradano rivers in Italy. A further case study, acquired on River Arrow in the UK was considered as a validation site. The choice of these field experiments incorporated the homogeneity of benchmark methods for surface velocity estimation (current meters), the presence of a high number of measurements, and a wider range of seeding conditions. Fig. 1a shows the different case studies' location and presents an example of the original grayscale frame for each case study (Fig. 1b - e). The main hydraulic and experimental settings are well documented in Perks et al., (2020b) and synthesised in Table 1.

The Brenta river campaign was carried out by Tauro et al. (2017) using a GoPro Hero3 + black edition camera mounted on a pole on the downstream side of a bridge and with a resolution of 1920 × 1080 px. The calibration factor from pixels to meters was estimated as 0.005 m/px. Reference measurements were acquired in-situ with an OTT Hydromet C2 current meter at four locations along the stream cross-section (see Fig. 1b). During the experiment, ten separate 20-second videos at 25 fps were recorded. However, due to some significant disturbances at the right side of the cross-section (light reflections on the water surface), the videos considered for this analysis were restricted to the first five sequences.

On the Noce river, Basilicata region (Italy), images were collected from a DJI Phantom 3 Pro UAS (Dal Sasso et al., 2018). A total of 400 consecutive images with a resolution of 1920x1080 px and a frame rate of 24 Hz were considered for the analysis. The ground sampling distance (GSD) was 0.009 m/px. Velocity measurements were acquired with a Seba F1 current meter at 13 locations spaced 1 m (see Fig. 1c).

The third case study is located in Bradano River, Basilicata region (Italy). Video footage was captured from a DJI Phantom 3 Pro UAS for 1 min 43 s at a pixel resolution of 1920x1080 px, and a frame rate of 24 Hz. Transformation of the images from pixel units to real metric world dimensions can be achieved using the following relationship: 1 px = 0.009 m. Benchmark velocities were obtained at seven points in the

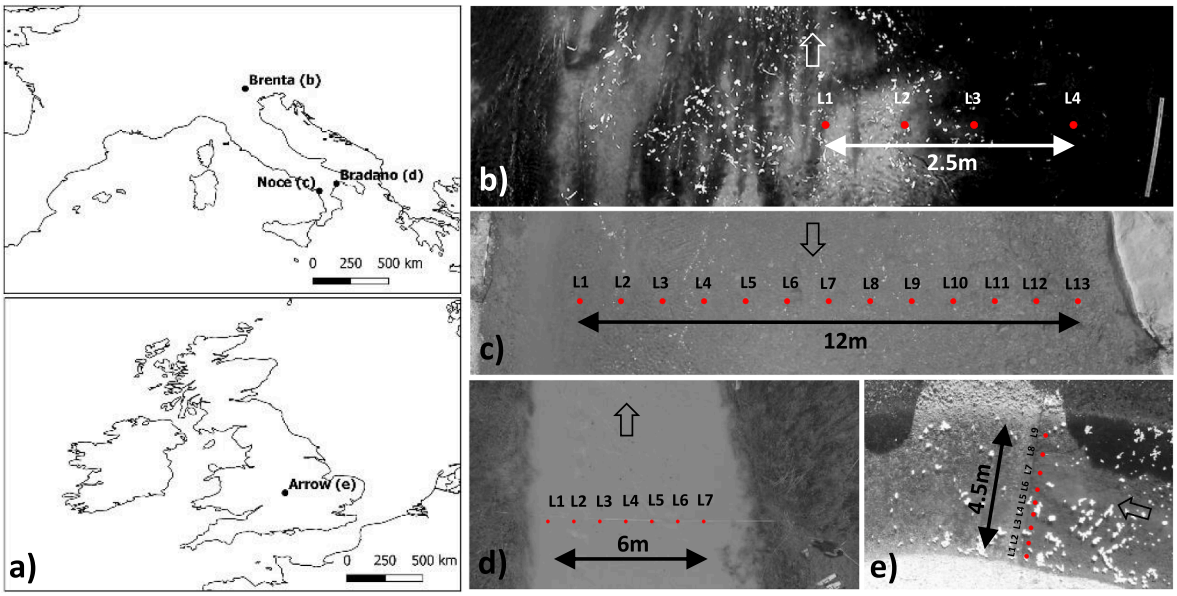

Fig. 1. a) Location of each case study with examples of frames captured with the indication of cross-section width monitored and measurement locations (red circles) distinguished in calibration dataset (b) Brenta river, Italy; c) Noce river, Italy; d) Bradano river, Italy) and e) validation dataset (Arrow river, UK). (For interpretation of the references to colour in this figure legend, the reader is referred to the web version of this article.)

Table 1
Main flow characteristics at monitored cross-sections with the description of image-based and current meter systems used for velocimetry purpose.

Case Study	Contributing Area [km^2]	Mean surface velocity [m/s]	Maximum surface velocity [m/s]	River discharge [m^3/s]	Image System	Benchmark measurements (n. locations)
Brenta (Italy)	252	0.38	0.46	2.76	fixed (bridge)	Current meter OTT Hydromet C2 (n.4)
Noce (Italy)	413	0.43	0.48	1.70	mobile (UAS)	Current meter SEBA F1 (n.13)
Bradano (Italy)	2581	0.82	1.47	3.97	mobile (UAS)	Current meter SEBA F1 (n.7)
Arrow (UK)	94	0.24	0.27	1.46	mobile (UAS)	Current meter Valeport 801 (n.9)

cross-section, at 1 m intervals, using a Seba F1 current meter (see Fig. 1d).

The River Arrow represents the case study considered for validation purposes which was acquired in Warwickshire, UK. Video footage was acquired using Phantom 4 Pro UAS with a pixel resolution 1920 × 1080 px and frame rate 30 Hz. The pixel dimensions of the processed imagery are 0.0096 m in the x and y axes. Reference measurements were obtained through a Valeport 801 electromagnetic current meter for two cross-sections within nine individual measurements with a spacing of 0.5 m between each (see Fig. 1e). The cross-section considered for the SDI and image velocimetry analysis was located upstream of the river bend. The latter has been done to minimise the effect of the bend on river velocity calculations.

For all the case studies, artificial seeding was manually deployed on the free surface upstream of the river reach monitored. In particular, wood chips were used on Brenta and Noce rivers, charcoal tracers on Bradano river, and eco foam chips on the River Arrow. Moreover, the discharge was calculated by applying the velocity-area method at velocity profiles sampled in the cross-sectional flow area (Herschy et al., 1985).

3. Materials and methods

For all the case studies, nadir videos were acquired with the camera's y-axis orthogonal to the flow direction. Therefore, no algorithm for orthorectification (distortion correction) was applied. However, videos captured by UAS were pre-processed to minimise the apparent movement of the platform. The stabilisation algorithm used consists of an automatic feature selection method that identifies features in frame pairs, matching them to compute possible camera movements (Dal Sasso et al., 2020, Pizarro et al., 2020b). The conversion between pixel units and metric units were done using Ground Control Points (GCP) targets or reference objects located in the field.

Videos were acquired at 24–30 frames per second (fps), and frames were extracted and resampled according to the average surface velocity measured in the field. The resampling is useful to enhance the particle displacement with respect to the tracer dimension and reduce computational time. In particular, for the Brenta river, the same frame rate used by Tauro et al. (2017) was adopted, which is 12.5 fps leading to a total number of 2500 frames to be analysed. The Noce river dataset was resampled at 12 fps according to the authors' analysis for a total of 400 frames (Dal Sasso et al., 2018). For the River Arrow, from the recordings, a dataset of 799 consecutive images (sampled at a frame rate of 5 Hz) were extracted for image velocimetry purposes. No resampling process was performed on the Bradano river because of the higher surface velocities measured in the field; therefore, the frame sequence comprised a total of 2496 frames.

The frames extracted were converted in grayscale intensity and pre-processed using binarisation to enhance lighter particles' visibility against a dark background as is required by the seeding metric tool (Pizarro et al., 2020b). Binarisation by thresholding converts the grayscale image (pixels values between 0 and 255) to an image with pixel

values of 0 and 1, by changing the foreground pixels to white and background pixels to black. To this aim, the binarisation threshold selected ranged between 80% and 90% of 255 (8 bits). A higher threshold (90%) was considered for the River Arrow because of the significant presence of light reflections during the frame footage. Table 2 contains all the video characteristics used for image-based analyses.

Afterwards, for each case study, the Seeding Distribution Index (SDI) (Pizarro et al. 2020a and 2020b) was calculated frame by frame and an SDI time series were produced. SDI is defined as:

$$SDI = D^{*0.1} / \left(\frac{\rho}{\rho_{cD^*1}} \right), \quad (1)$$

where $D^*, \rho,$ and ρ_{cv1} are the empirical spatial clustering level of tracers, the seeding density, and the converging seeding density at the Poisson case (D*=1), respectively. ρ_{cD^*1} was estimated as 1.52E−03 particles per pixel (ppp) in Pizarro et al. (2020b), whereas D* is computed as [Var (N)/E(N)], where Var(N) and E(N) are the spatial variance and mean value of the number of tracers N computed on subsectors of the same dimensions. It is critical to underline that SDI showed a strong positive correlation with velocimetry errors. Therefore, it can be used as a proxy to select the best set of images for image velocimetry applications.

The spatial distribution of tracers varies significantly along the cross-section producing different seeding configurations in time and space. This variability depends on different aspects: the hydrodynamic characteristic of the flow, the morphological characteristics of the river reach, the type and amount of material deployed, and the number and experience of operators. For this reason, SDI time-series calculations and LSPIV analyses were performed at the cross-section scale (sector scale) and at sub-portions (sub-sector scale), as illustrated in Fig. 2. Different Region of Interests (ROIs) were identified, consisting in one sector covering the entire transect of benchmark measurements and two sub-sectors of the same dimension, located in the left (LH) and right (RH) part of the cross-section. In particular, the ROI was schematised as a rectangle with one size equal to benchmark measurements (along the cross-section) and the other size of 1 m (along the flow direction). For the Bradano river case study, a more extended ROI was considered (about 4 m in the flow direction) to allow statistical analysis inside the ROIs because of the low seeding conditions. Fig. 2 shows a schematic representation of the cross-section of the Bradano river with the entire sector and two sub-sectors considered for the analysis.

Starting from SDI time-series calculations (Fig. 3a), a smoothing function was applied to the SDI time series to reduce the noise. This function uses the moving average filter that smooths data by replacing each data point with the average of the neighbouring data points defined within the span of 10 frames (Fig. 3b). The filtered SDI time-series average value was considered a threshold to identify the best video portion to analyse. The used criteria are based on: *1)* the identification of frames with an SDI index lower than the average threshold; *2)* the selection of the best frame window (FW) that maximises the number of frames; and if more than one FW assures 1 and 2, a further criterion applies. This criterion relies on the minimisation of the SDI averaged within the frame window (Fig. 3c).

LSPIV analysis was carried out using the PIVLab software (Thielicke and Stamhuis, 2014), an open-source toolbox for image velocimetry analysis developed in Matlab. The LSPIV algorithm was applied using the Fast Fourier Transform (FFT) with a three-pass standard correlation method (search and interrogation areas of 128 × 64, 64 × 32, and 32 × 16 px). Additionally, the 2 × 3-point Gaussian fit was employed to estimate the sub-pixel displacement peak. This method fits a one-dimensional Gaussian function to the discrete intensity distribution of the correlation matrix to determine the sub-pixel particle displacement. The images were analysed adopting the sequencing style 1–2, 3–4. This choice led to optimising the analysis for video sequences (e.g., Brenta river) in which non-consecutive frames between videos were available. Moreover, no post-processing method was applied to filter erroneous velocity results.

Table 2
Main video characteristics after pre-processing.

Case Study	GSD [m/px]	fps	Number of Frames	Binarisation [%]
Bradano (Italy)	0.009	24	2496	80
Brenta (Italy)	0.005	12.5	1250	80
Noce (Italy)	0.009	12	200	80
Arrow (UK)	0.0096	5	799	90

The performance of LSPIV results was determined by comparing for each measurement location (i) the computed velocities with the current meter measurements considering only the component of velocity in the flow direction (U). Velocity values of each location represent the average of velocity estimated in a square with sides of 0.30 m centred on the measured point (Dal Sasso et al., 2018).

The Absolute Percentage Error, APE_i (where i refers to the generic measurement location) was calculated as:

$$APE_i = \left| \frac{(U_{Ci} - U_{Ri})}{U_{Ri}} \right| \% \quad (2)$$

where U_{Ci} is the computed velocity and U_{Ri} is the reference velocity.

For each case study, the index *MAPE* (Mean Absolute percentage error), that is the mean of all the APE_i, was calculated as:

$$MAPE = \frac{1}{n} \sum_{1=1}^{n} APE_i = \frac{1}{n} \sum_{1=1}^{n} \left| \frac{(U_{Ci} - U_{Ri})}{U_{Ri}} \right| \% \quad (3)$$

where n refers to the total number of measurement locations.

4. Results

In this section, we report the results of the application of the method illustrated previously. We first present the SDI calculation for each case study at sector and sub-sector scales identifying the frame window (FW) that satisfies the criteria described in Section 2.2. Then, we show the image velocimetry results obtained by analysing all video data available and the best frame window identified after SDI calculation. A unique empirical threshold is identified and applied to a validation case study to test the benefits of the method proposed. Finally, we compare the velocity estimations from LSPIV to the benchmark measurements at different local scales to estimate mean absolute errors.

4.1. SDI time series analysis

Fig. 4 shows an overview of the dimensionless SDI index calculated for the entire ROI and two sub-sectors, located on the left (LH) and the right part (RH) of the cross-sections, respectively. Note that LH and RH are defined considering the flow direction.

The Brenta river presented the highest seeding density values (2.75E−03 ppp) and spatial distribution of tracers (14.31). The behaviour of the SDI along the frame footage was very stable (between 0.35 and 1.34) especially in the left part of the cross-section similar to the entire sector (Fig. 4a, b). On the contrary, the SDI time series referred to the RH sub-sector showed a different behaviour due to the lower seeding density that reached an average value of 7.93E−04 ppp (Fig. 4c). On the Noce river, the average seeding density calculated was 7.70E−04 ppp, and the spatial distribution of tracers was 6.96. The SDI values along the video footage were more consistent and showed the highest variability (between 1.63 and 5.61). On the Brenta river, the behaviour of the SDI in the left part of the cross-section was similar to the entire sector while in the right sub-sector was quite different (Fig. 4d,e,f). The Bradano River had the lowest seeding values (6.89E−05 ppp) and the dispersion of tracers (2.80). As showed in Fig. 4g, the SDI values showed the highest variability (between 7.19 and 390.24). This variability was particularly evident in the left part of the cross-section where the lack of seeding did

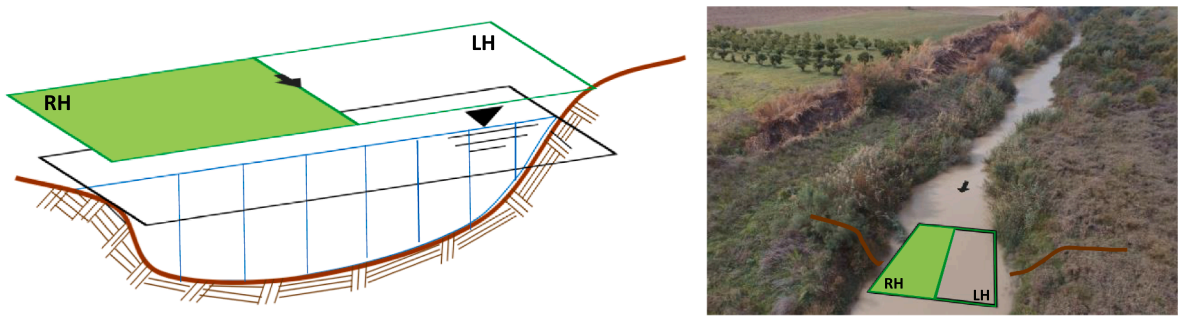

Fig. 2. Schematic representation of cross-section on Bradano river (Italy) with an indication of the sector (black box) and sub-sectors (green boxes) for the SDI calculations and image velocimetry analysis. (For interpretation of the references to colour in this figure legend, the reader is referred to the web version of this article.)

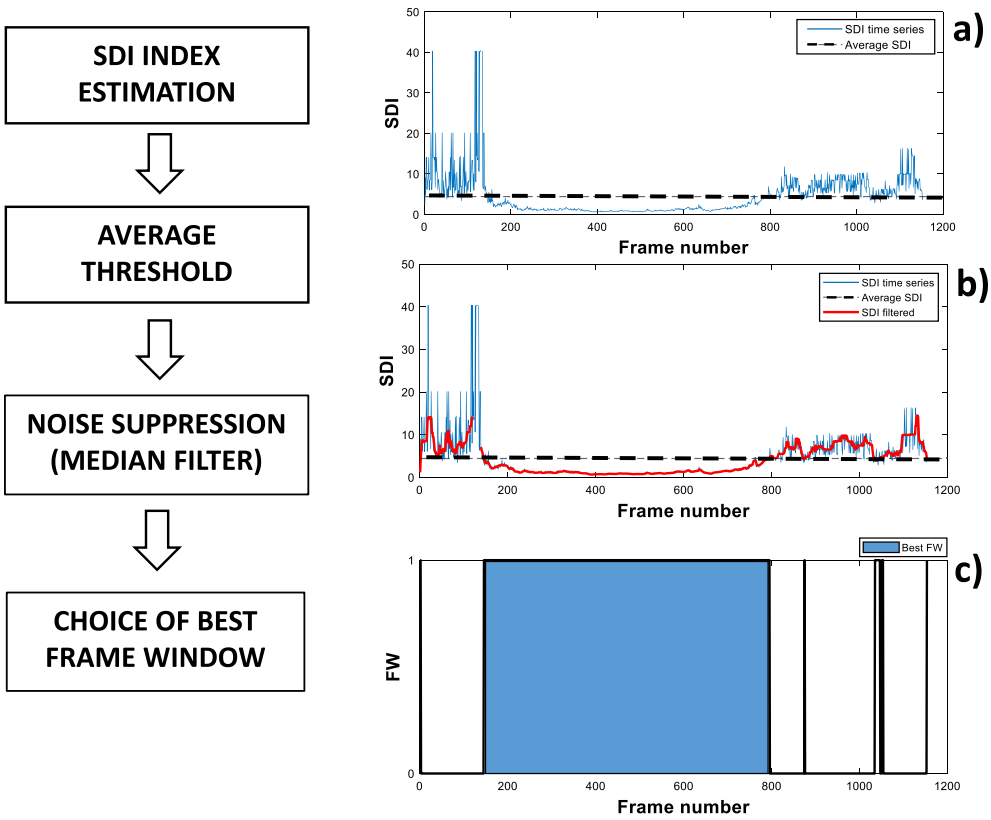

Fig. 3. The methodology used includes the following three steps: a) SDI time series and average SDI calculation (dashed line); b) SDI filtering (red line); c) individuation of the best frame window (light blue box). (For interpretation of the references to colour in this figure legend, the reader is referred to the web version of this article.)

not allow the calculation of SDI values for different frames in the last part of the video (Fig. 4h).

Fig. 5 shows the surface velocity maps computed for the three case studies considering the entire video configuration and the best one between one and two sectors. From this figure, it is possible to observe that a good sampling of velocities inside the ROIs is generally obtained also reducing the number of frames processed (e.g., 6% of the total frames in Brenta river). This depends on the SDI behaviour inside the ROI, increasing its influence at low seeding conditions (e.g., Bradano river). Note that a great level of detail is achieved in Fig. 5 even with a reduced – but highly informative – number of frames. This idea is validated considering the case study below.

Table 3 presents the average values of seeding density ($\overline{\rho}$), dimensionless dispersion index ($\overline{D}^*$), and SDI threshold for each case study at the sector and sub-sectors scales. Moreover the $\tau = \rho_{cD^*1}\overline{D}^{*0.1}$ parameter was calculated. It is worth noting that τ represents a key factor to derive the SDI threshold using only seeding density information. We observed that on average this parameter stabilised around 0.002 ppp when tracers transit in the field of view for the different case studies considered in this work. In contrast, it increased when the video footage includes frame sequences without seeding (e.g. Bradano, LH sub-sector).

4.2. Image velocimetry results

Table 4 presents the summarised information about the comparison of LSPIV velocity estimates and the current meter measurements for each case study. MAPE is presented for the different configurations that include the analysis considering all the frames and adopting the optimal frame window for one sector and two sub-sectors. The error reduction,

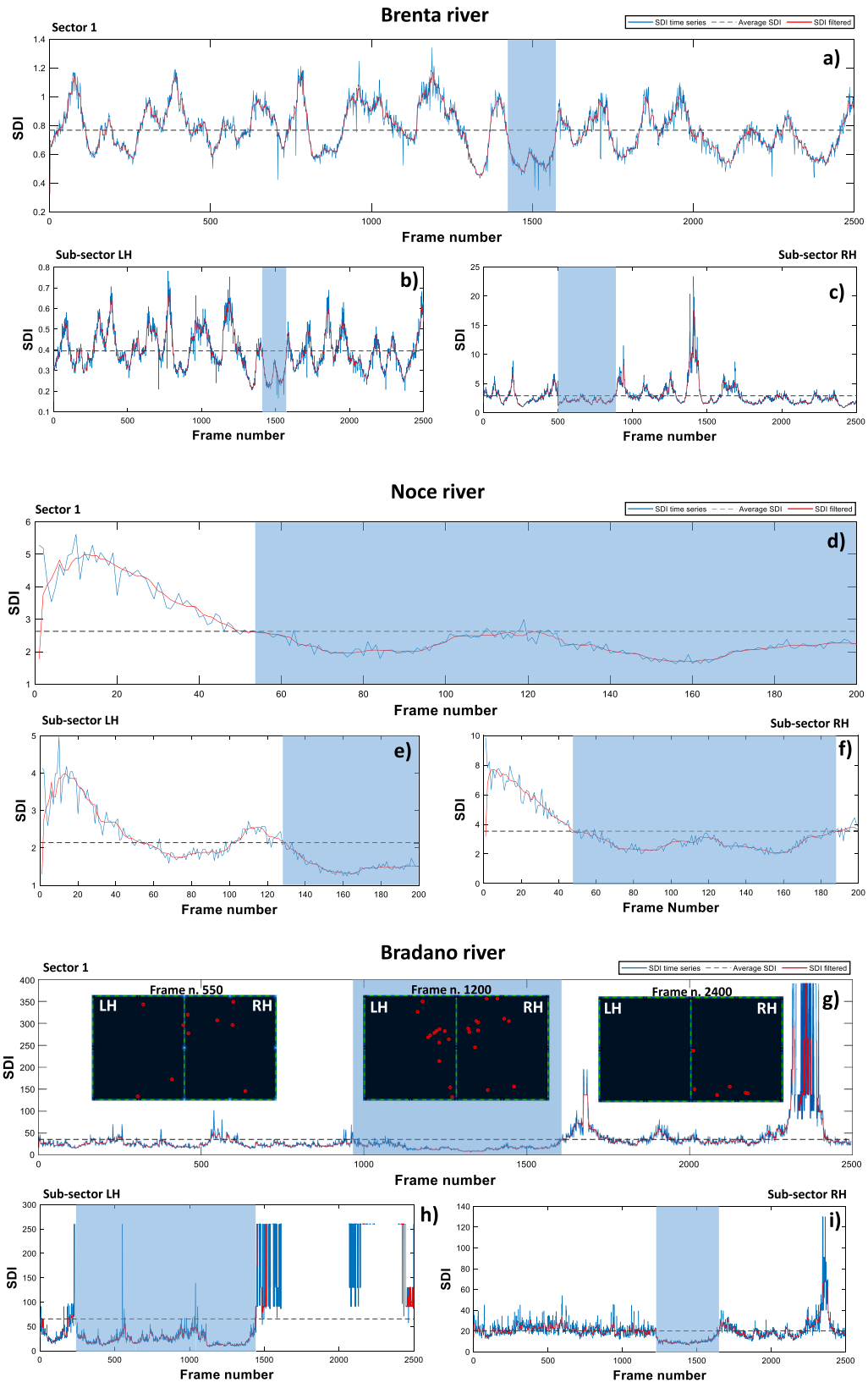

Fig. 4. SDI times series calculated at sector and sub-sectors scales (LH and RH are the left-hand and right-hand subsectors) with the indication of the SDI threshold (dashed line) and best frame window (light blue box) for a,b,c) Brenta river; d,e,f) Noce river; and g,h,i) Bradano river, respectively. The red line represents the filtered SDI time series. (For interpretation of the references to colour in this figure legend, the reader is referred to the web version of this article.)

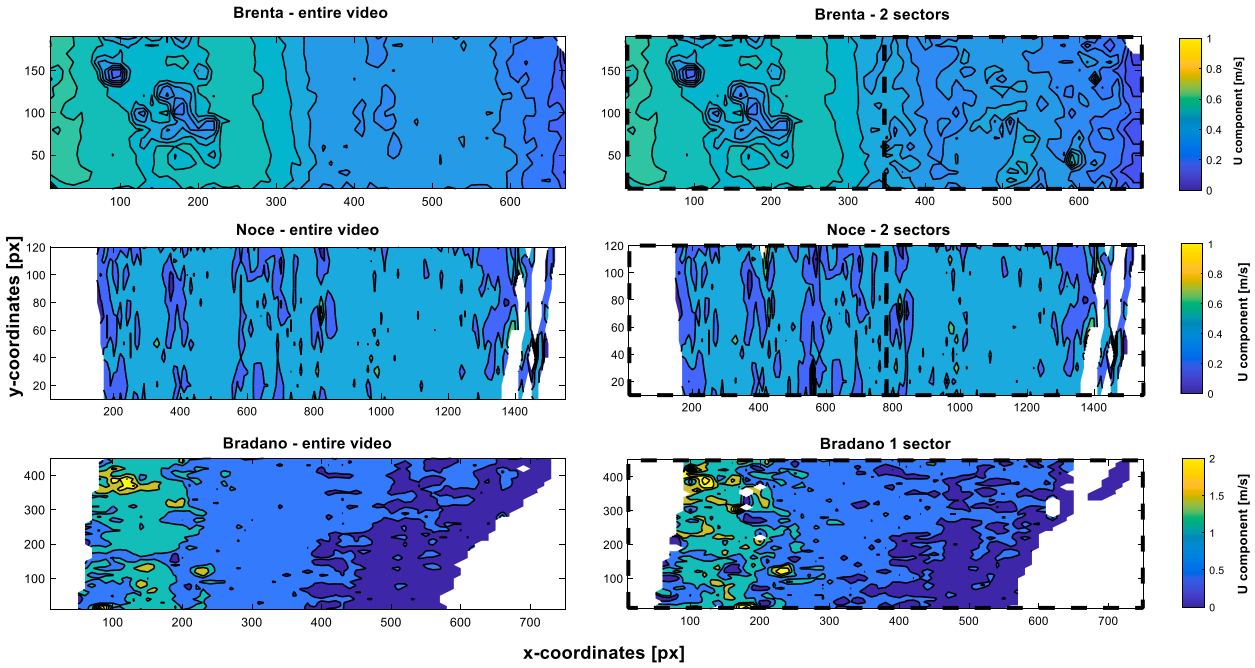

Fig. 5. Averaged surface velocity maps computed for each study case inside the ROI considering the entire video and the best configuration between the entire ROI or two sub-sectors (dashed black boxes).

Table 3
Average seeding characteristics, expressed in terms of average seeding density ($\bar{\rho}$), spatial distribution of tracers ($\overline{D}^*$), SDI threshold and parameter (τ), calculated at sector and sub-sector scales for the calibration dataset.

River	Number of sectors	$\bar{\rho}$ [ppp]	$\overline{D}^*$ [–]	SDI threshold [–]	τ[ppp]
Brenta	1	2.75E-03	14.31	0.77	0.0021
	2-LH	4.98E-03	7.06	0.36	0.0018
	2-RH	7.93E-04	7.12	2.89	0.0023
Noce	1	7.70E-04	6.96	2.62	0.0020
	2-LH	9.52E-04	7.02	2.14	0.0020
	2-RH	5.91E-04	6.18	3.54	0.0021
Bradano	1	6.89E-05	2.8	30.72	0.0021
	2-LH	5.00E-05	2.17	60.72	0.0030
	2-RH	9.42E-05	2.28	20.99	0.0020

Table 4
Overview of average absolute errors calculated considering all the frames and the best frame windows over the entire ROI and sub-sector scales. Values in parenthesis represent the reduction of error in percentage respect to the configuration adopting all frames on the entire ROI or specific sector, respectively.

River	Sectors	Number of frames n	Frame window	MAPE [%]	
Brenta	1	2500	entire video	14.26%	
	1	154	1420–1573	13.92% (−2%)	
	2-LH	2500	entire video	13.30%	
	2- RH	2500	entire video	15.22%	
	2-LH	154	1420–1573	7.26% (−45%)	10.88%
	2- RH	379	501–879	14.49% (−5%)	(−24%)
Noce	1	201	entire video	14.28%	
	1	150	52–201	11.44% (−20%)	
	2-LH	201	entire video	17.40%	
	2- RH	201	entire video	10.63%	
	2-LH	71	130–201	10.07% (−42%)	9.92%
	2- RH	124	48–186	9.27% (−13%)	(−31%)
Bradano	1	2496	entire video	12.23%	
	1	642	967–1608	9.34% (−24%)	
	2-LH	2496	entire video	15.82%	
	2- RH	2496	entire video	9.84%	
	2-LH	1194	250–1443	10.63% (−28%)	11.06%
	2- RH	422	1224–1645	10.28% (+4%)	(−9%)

expressed in terms of MPE, obtained using the best frame window with respect to the entire video configurations are reported in brackets, for both one and two sectors. Appendix A synthesises, for each case study, the following information: a reference pre-processed image with the indication of current meter measurements (L_i) and the two sub-sectors (LH and RH), the reference surface velocities, and absolute percentage error APE (%) calculated for each location considered in the analysis.

For all the case studies, a reduction of absolute percentage error was found by employing the optimal frame window that minimises SDI at different spatial scales. In particular, on the Brenta river, the MAPE considering all the available frames (n = 2500) was equal to 14.26%; moving on, the best frame window in the sector (n = 154 frames) stabilised around 13.92% with an error reduction of 2%. The restricted number of frames considered for the LSPIV analysis determined an improvement of the results on the left side (locations L1 and L2) compared to the right side characterised by a lower seeding density (see location L3, see Table A1 in Appendix A). Considering the different SDI behaviours inside the two sub-sectors, the LSPIV results stabilised with an error of around 10.88%, leading to an overall error reduction of 24%. On the Noce river, MAPE was 14.28% considering all the frames available (n = 201). Despite the low number of frames analysed, the high seeding density allowed the selection of an optimised frame window to improve the final results on both the sector and sub-sector scales. The errors calculated using the best FW in one sector and two sectors were 11.44% and 9.92% with an error reduction of 20 and 31%, respectively. On the Bradano river, the high number of frames allowed the

applicability of the methodology in extremely low seeding conditions. The average absolute error computed using all frames (n = 2496) was 12.23%, whereas considering the best frame window at one sector was 9.34% with a reduction of 24%. No significant improvement was found using the best frame window at sub-sector scales (11.06%). The latter can be explained by the limited number of frames analysed in the right portion of the cross-section because of the lower seeding density and sampled velocity vectors which are not enough to reconstruct the velocity field accurately.

4.3. Validation on the river arrow

The River Arrow dataset, described in Section 2.1, has been used for the validation of the proposed procedure (Fig. 6). In particular, the empirical threshold $\tau = 0.002$ ppp, calibrated on the other three study cases, was tested to identify the best temporal frame window for image-velocimetry analyses. The River Arrow case study showed high average seeding density (7.37E−04 ppp) and low dispersion of tracers in the field of view (2.72).

The seeding behaviour was similar inside the different sectors because of the homogeneous distribution of tracers on the mid-cross-section (Fig. 7a, b, c). However, more noise effect was visible in the sector in the right part of the cross-section (Fig. 7c). Considering the parameter $\tau = 0.002$ ppp and the reference seeding density for each sector, the calculated SDI thresholds were equal to 2.71 (sector 1), 1.82 (sub-sector LH) and 3.70 (sub-sector RH).

These thresholds allowed the identification of the best frame windows within the video footage and image velocimetry analysis was performed using only these frames (Table 5). The mean absolute percentage error computed using all frames available (n = 798) over the entire ROI was 12.37%; whereas using the best frame window (n = 282) the error reduced by around 7.59%. In the present case, the analysis performed on the two subsectors was not able to identify a significantly different set of frames. For this reason, the error was similar to the one performed over the entire ROI with an error of around 8%. This is due to the fact that seeding distribution is quite uniform in space.

Fig. 8 shows the surface velocity map computed considering the entire video and the optimal frame window. It is possible to observe that the homogeneous seeding conditions allowed to obtain a full velocity map with a significantly reduced error using about 35% of the total number of frames. In the present case, the optimal velocity map retained was the one estimated over the entire ROI, because we measured an increase in errors on the right sector with respect to the current meter. It is worth noting the error in the two subsectors obtained using the optimal set of frames is below 8.4%, while the same result obtained including all frames shows a variability from 5.15% up to 19.63%. Notwithstanding the uncertain reliability of the current meter data, it is important to acknolwedge the results obtained on the two subsectors provide a more stable result, which opens the possibility of improving image velocimetry methods' reliability and accuracy.

Fig. 6. River Arrow with the indication of the cross-section monitored upstream the bend and the two ROIs considered for the analysis.

5. Discussion

The accuracy of image velocimetry techniques strongly depends on the occurrence of visible features (e.g., boils, surface ripples, vegetation debris) on the water surface. In a natural environment, the amount, spatial distribution, and visibility of natural features at the river surface are continuously changing because of environmental factors (reflections, shadows, wind, rain) and hydraulic conditions (water ripples, hydraulic jumps, and standing waves). For this reason, the actual seeding in the field is not always properly captured by the post-processed images (Dal Sasso et al., 2020). In practice, tracers may vary in amount, organisation, and even presence/absence during field experiments or natural conditions. Therefore, operators frequently add traceable particles to increase the accuracy and reliability of the surface velocity measurements. However, also in this case, floating natural particles could not cover the entire observed cross-section, leading to data gaps or near-zero velocities (e.g., typically near the banks).

To avoid these issues and answer to these practical difficulties, in this work a method based on an SDI threshold is proposed to define the best seeding conditions inside a frame sequence. This approach uses only the frames with an SDI below a given threshold, reducing the investigation scale at sub-sectors to maximise this information. The method was applied to different case studies characterised by different lengths of videos and specific seeding conditions in space and time. The SDI-based method improved LSPIV performance with a reduction of image velocimetry errors ranging between 2 and 39% depending on the variability of SDI time series along the frame sequence. These improvements are even more evident at sub-sector scales, when a different seeding behaviour was observed, allowing the possibility to select frames with tracers continuously visible across the ROI. At this scale, a significant reduction of error, between 24 and 33%, was found on the Brenta and Noce rivers respectively. The application of the method at the sector and sub-sector scales allowed a full velocity map to be obtained with a significant reduction in computational time for the analysis, reducing the number frames processed. Moreover, in such cases, the average surface velocity maps contain details (e.g., velocity fluctuations and divergences) that are not visible and appreciable in the entire video configuration (see, i.e., Brenta and Noce case studies, on RH and LH sectors respectively). The empirical parameter $\tau = \rho_{cD^*1} D^{*0.1}$ calibrated on three case studies could be particularly useful to derive SDI thresholds and the best frame window from the unique information on seeding density. On average, this parameter stabilised around 0.002 ppp in the circumstances in which seeding was visible inside the ROI and tended to increase for videos only when tracers were not observable. Comparing the LSPIV results with reference measurements in all the case studies, the mean absolute average error computed was around 8–10%. Except for the Brenta where a systematic overestimation of velocities was found, in general, LSPIV results tend to underestimate surface flow velocities, especially for the areas close to the river banks, where fewer tracers were observed.

The SDI threshold can represent an efficient method for searching the best frame window to analyse within the video footage. This is feasible when the number of frames inside the FW identified is adequate to perform analysis with enough vector samples. This information is strongly related to the effective seeding detected by the image velocimetry technique, and its recognition is particularly critical in low seeding conditions. A high number of uniformly distributed particles allows a reduction in the number of frames to analyse; on the contrary, a low seeding density requires a higher number of frames to obtain consistent improvements and full surface velocity maps (e.g. the Bradano river).

The proposed method could be particularly useful for analysing a long sequence of frames or multiple videos recorded from a fixed monitoring station, facilitating the generation of time series for image

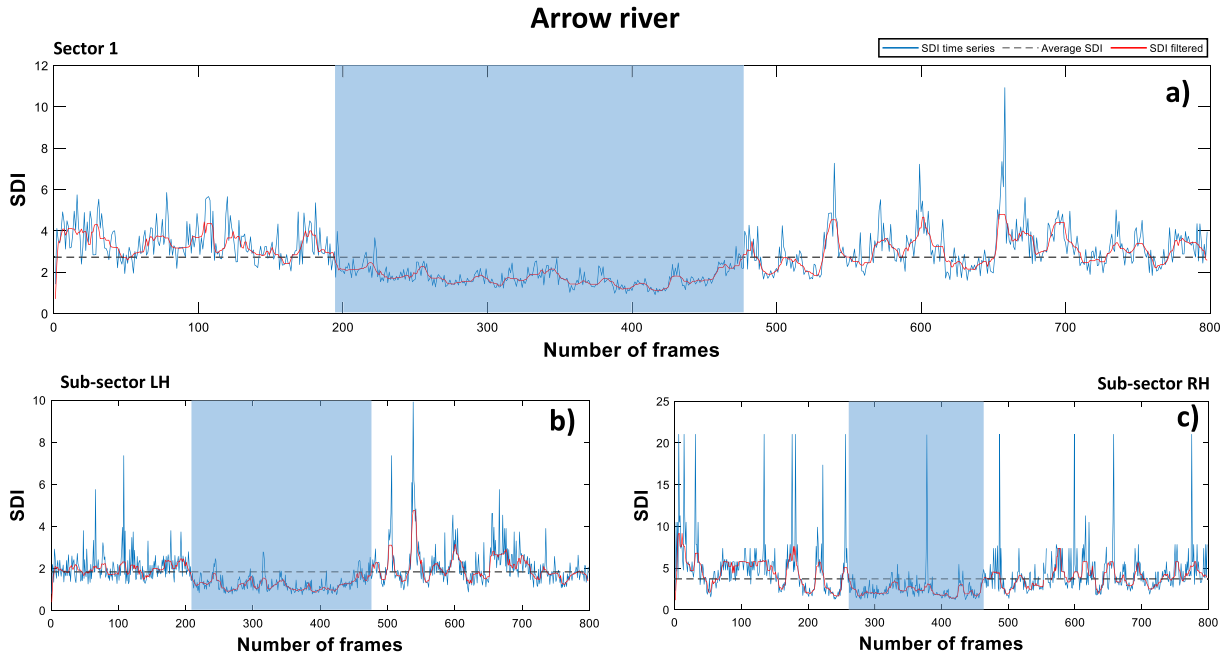

Fig. 7. SDI time series calculated on Arrow river at sector and sub-sectors scales (LH and RH) with the indication of SDI threshold (dashed line) and best frame window (light blue box). (For interpretation of the references to colour in this figure legend, the reader is referred to the web version of this article.)

Table 5
Average absolute errors calculated considering all the frames and the best frame windows over the entire ROI and sub-sector scales for the River Arrow. Values in parenthesis represent the reduction of error in percentage respect to the configuration adopting all frames on the entire ROI or specific sector, respectively.

River	Sectors	Number of Frames	Frame Window	MAPE [%]	
Arrow	1	798	entire video	12.37%	
	1	282	195–476	7.59 (−39%)	
	2-LH	798	entire video	19.63%	
	2- RH	798	entire video	5.15%	
	2-LH	270	206–475	8.16% (−58%)	8.01
	2- RH	202	262–463	8.37% (+62%)	(−33%)

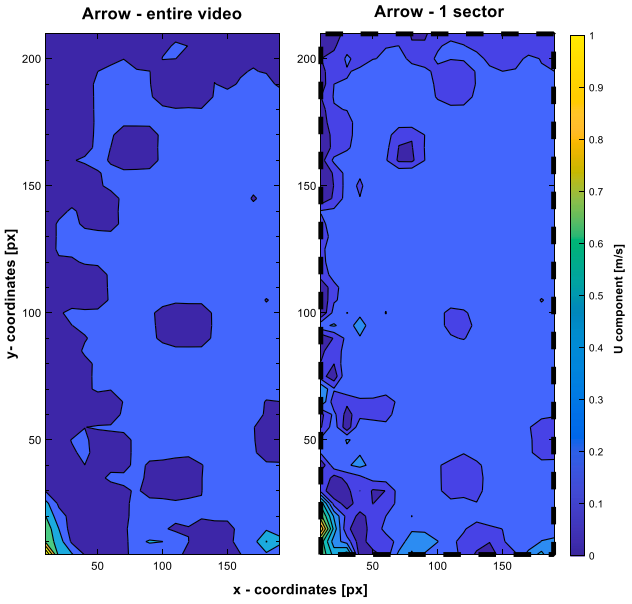

Fig. 8. Averaged surface velocity map computed for Arrow river inside the ROI considering the entire video and the one sector configuration.

velocimetry analysis. One of the most important limitations of the image velocimetry techniques, especially for traditional correlation-based methods, is the computational time. The detection of the best frame window can minimise the number of frames to analyse, reducing computational loads. The latter can be extremely useful for gauge-cams that can directly process the images in situ without the occurrence of additional drives for storing image sequences (Tosi et al., 2020). Moreover, the application of the method at a local scale can be particularly suited for image velocimetry analysis of flood events where the best seeding conditions are particularly challenging. Its application can be interesting at large rivers in which seeding is generally sparse and completely absent for long frame sequences. More sectors would be identified in these cases to specify image velocimetry analysis only inside the best frame windows. It is worth noting that numerous water reflections appearing as tracers in the field of view represent one of the most important factors that can negatively influence the use of the SDI methods. An increase of apparent seeding density and the reduction of the SDI index can strongly affect image velocimetry results, producing erroneous reconstructions of the flow field. This issue can be frequent in natural environments where the conditions are challenging and could be alleviated through extensive image pre-processing. A greater effort is necessary in this direction in our vision, identifying a set of strategies to automatically discriminate tracers from water reflections and environmental noise in natural settings.

6. Conclusion

In this work, a novel method for the identification of the optimal spatial structure of tracers was introduced to strengthen surface velocity estimation in natural rivers. The approach uses a threshold for selecting the best frame window (FW) based on the SDI values. SDI time series were calculated at the sector and sub-sector scales of each cross-section in order to investigate the scale impact on the proposed seeding metrics. Analyses highlighted that the proposed procedure might improve the overall LSPIV results with an average reduction of velocity errors of between 20% and 39%. Moreover, we observed that the seeding

density's calibrated thresholds remain relatively stable around a value of 0.002 ppp, which can be used as a reference quality measure of an image containing tracers. This value was, in fact, successfully applied to the validation study case of the River Arrow.

The method appears suitable for natural settings where environmental and hydraulic conditions are extremely challenging and particularly useful for real-time implementations on gauge-cams, where a vast number of frames is usually recorded and analysed. Reducing the observation scale for image velocimetry analysis is a novel idea, successfully explored in this work that reveals a high potential for applying other image velocimetry techniques. In future, this method will be tested on other case studies considering additional seeding configurations and environmental conditions.

7. Code availability statement

The code used to define the best frame window is available at https://doi.org//10.17605/OSF.IO/3AJNR (Dal Sasso et al., 2021). The code used to compute the SDI index as well as seeding metrics is available at https://doi.org/10.17605/OSF.IO/8EGQW.

8. Data availability statement

The data that support the findings of this study are openly available in 4TU.Centre for Research Data at https://doi.org/10.4121/uuid:014d56f7-06dd-49ad-a48c-2282ab10428e (Perks et al., 2020b).

Funding

This research was funded by COST Action CA16219, "HARMONIOUS-Harmonization of UAS techniques for agricultural and natural ecosystems monitoring". Data analysed for the River Arrow study was collected as part of a University of Worcester PhD studentship.

Declaration of Competing Interest

The authors declare that they have no known competing financial interests or personal relationships that could have appeared to influence the work reported in this paper.

Appendix A. Supplementary data

Supplementary data to this article can be found online at https://doi.org/10.1016/j.jhydrol.2021.126438.

References

Bandini F, Lüthi B, Peña-Haro S, Borst C, Liu J, Karagkiolidou S, Hu X, Lemaire GG, Bjerg PL, Bauer-Gottwein P 2020. A drone-borne method to jointly estimate discharge and Manning's roughness of natural streams. Water Resources Research. DOI:10.1029/2020WR028266.

Brevis, W., Niño, Y., Jirka, G.H., 2011. Integrating cross-correlation and relaxation algorithms for particle tracking velocimetry. Exp. Fluids 50 (1), 135–147.

Dal Sasso, S.F., Pizarro, A., Pearce, S., Maddock, I., Manfreda, S., 2021. Increasing LSPIV performances by exploiting the seeding distribution index at different spatial scales (Version 0.1). [codes] OSF. DOI:10.17605/OSF.IO/3AJNR.

Dal Sasso, S.F., Pizarro, A., Samela, C., Mita, L., Manfreda, S., 2018. Exploring the optimal experimental setup for surface flow velocity measurements using PTV. Environ. Monit. Assess. 190 (8) https://doi.org/10.1007/s10661-018-6848-3.

Dal Sasso, S.F., Pizarro, A., Manfreda, S., 2020. Metrics for the quantification of seeding characteristics to enhance image velocimetry performance in rivers. Remote Sens. 12 (11), 1789. https://doi.org/10.3390/rs12111789.

Detert, M., Johnson, E.D., Weitbrecht, V., 2017. Proof-of-concept for low-cost and non-contact synoptic airborne river flow measurements. Int. J. Remote Sens. 38 (8-10), 2780–2807.

Eltner, A., Sardemann, H., Grundmann, J., 2020. Technical Note: Flow velocity and discharge measurement in rivers using terrestrial and unmanned-aerial-vehicle imagery. Hydrology and Earth System Sciences 24.

Fujita, I., Muste, M., Kruger, A., 1998. Large-scale particle image ve-locimetry for flow analysis in hydraulic engineering applications. J. Hydraul. Res. 36 (3), 397–414.

Fujita, I., Watanabe, H., Tsubaki, R., 2007. Development of a non-intrusive and efficient flow monitoring technique: the space-time image velocimetry (STIV). Int. J. River Basin Manage. 5 (2), 105–114.

Herschy, R.W., 1985. Streamflow measurement, Elsevier Applied Science Publishers.

Kim, Y., Muste, M., Hauet, A., Krajewski, W.F., Kruger, A., Bradley, A., 2008. Stream discharge using mobile large-scale particle image velocimetry: a proof of concept. Water Resour. Res. 44, W09502. https://doi.org/10.1029/2006WR005441.

Kinzel, P.J., Legleiter, C.J., 2019. sUAS-based remote sensing of river discharge using thermal particle image velocimetry and bathymetric lidar. Remote Sensing 11 (19), 2317.

Le Boursicaud, R., Pénard, L., Hauet, A., Thollet, F., Le Coz, J., 2016. Gauging extreme floods on YouTube: application of LSPIV to home movies for the post-event determination of stream discharges. Hydrol. Processes 30 (1), 90–105. https://doi.org/10.1002/hyp.10532.

Le Coz, J., Hauet, A., Pierrefeu, G., Dramais, G., Camenen, B., 2010. Performance of image-based velocimetry (LSPIV) applied to flash-flood discharge measurements in Mediterranean rivers. J. Hydrol. 394 (1-2), 42–52. https://doi.org/10.1016/j.jhydrol.2010.05.049.

Leitão, J.P., Peña-Haro, S., Lüthi, B., Scheidegger, A., Moy de Vitry, M., 2018. Urban overland runoff velocity measurement with consumer-grade surveillance cameras and surface structure image velocimetry. J. Hydrol 565, 791–804.

Manfreda, S., McCabe, M., Miller, P., Lucas, R., Pajuelo Madrigal, V., Mallinis, G., Ben Dor, E., Helman, D., Estes, L., Ciraolo, G., Müllerová, J., Tauro, F., de Lima, M., de Lima, J., Maltese, A., Frances, F., Caylor, K., Kohv, M., Perks, M., Ruiz-Pérez, G., Su, Z., Vico, G., Toth, B., 2018. On the use of unmanned aerial systems for environmental monitoring. Remote Sens. 10 (4), 641. https://doi.org/10.3390/rs10040641.

Manfreda, S., Dvorak, J., Mullerova, S., Herban, P., Vuono, J.J.A., Justel, M.P., 2019. Assessing the accuracy of digital surface models derived from optical imagery acquired with unmanned aerial systems. Drones 3 (1), 15. https://doi.org/10.3390/drones3010015.

Manfreda, S., Dal Sasso, S.F., Pizarro, A., Tauro, F., 2019b. New Insights Offered by UAS for River Monitoring. In Applications of Small Unmanned Aircraft Systems: Best Practices and Case Studies.

Muste, M., Fujita, I., Hauet, A., 2008. Large-scale particle image velocimetry for measurements in riverine environments. Water Resour. Res. 44 (4) https://doi.org/10.1029/2008WR006950.

Pearce, S., Ljubičić, R., Peña-Haro, S., Perks, M., Tauro, F., Pizarro, A., Dal Sasso, S., Strelnikova, D., Grimaldi, S., Maddock, I., Paulus, G., Plavšić, J., Prodanović, D., Manfreda, S., 2020. An evaluation of image velocimetry techniques under low flow conditions and high seeding densities using unmanned aerial systems. Remote Sens. 12 (2), 232. https://doi.org/10.3390/rs12020232.

Perks, M.T., 2020. KLT-IV v1.0: image velocimetry software for use with fixed and mobile platforms. Geosci. Model Dev. 13, 6111–6130. https://doi.org/10.5194/gmd-13-6111-2020.

Perks, M.T., Dal Sasso, S.F., Hauet, A., Jamieson, E., Le Coz, J., Pearce, S., Peña-Haro, S., Pizarro, A., Strelnikova, D., Tauro, F., Bomhof, J., Grimaldi, S., Goulet, A., Hortobágyi, B., Jodeau, M., Käfer, S., Ljubičić, R., Maddock, I., Mayr, P., Paulus, G., Pénard, L., Sinclair, L., Manfreda, S., 2020a. Towards harmonisation of image velocimetry techniques for river surface velocity observations. Earth Syst. Sci. Data 12 (3), 1545–1559. https://doi.org/10.5194/essd-12-1545-2020.

Perks, M., Sasso, S.F., (Silvano FD, Detert M (Martin), Hauet A (Alexandre), Jamieson E (Elizabeth), Coz J (Jérôme) Le, Pearce S (Sophie), Peña-Haro S (Salvador), Pizarro A (Alonso), Strelnikova D, et al., 2020b. Data on the harmonization of image velocimetry techniques, from seven different countries, , DOI: 10.4121/uuid:014d56f7-06dd-49ad-a48c-2282ab10428e.

Pizarro, A., Dal Sasso, S.F., Manfreda, S., 2020a. Refining image-velocimetry performances for streamflow monitoring: Seeding metrics to errors minimisation, Hydrological Processes, (doi: 10.1002/hyp.13919), 1-9, 2020a.

Pizarro, A., Dal Sasso, S.F., Perks, M.T., Manfreda, S., Manfreda, S., 2020b. Identifying the optimal spatial distribution of tracers for optical sensing of stream surface flow. Hydrol. Earth Syst. Sci. 24 (11), 5173–5185. https://doi.org/10.5194/hess-24-5173-2020.

Rozos, E., Dimitriadis, P., Mazi, K., Lykoudis, S., Koussis, A., 2020. On the uncertainty of the image velocimetry method parameters. Hydrology 2020 (7), 65.

Samarage, C.R., Carberry, J., Hourigan, K., Fouras, A., 2012. Optimisation of temporal averaging processes in PIV. Exp. Fluids 52 (3), 617–631. https://doi.org/10.1007/s00348-011-1080-8.

Strelnikova, D., Paulus, G., Käfer, S., Anders, K.-H., Mayr, P., Mader, H., Scherling, U., Schneeberger, R., 2020. Drone-Based optical measurements of heterogeneous surface velocity fields around fish passages at hydropower dams. Remote Sens. 12 (3), 384. https://doi.org/10.3390/rs12030384.

Tauro, F., Piscopia, R., Grimaldi, S., 2017. Streamflow observations from cameras: large-scale particle image velocimetry or particle tracking velocimetry? Water Resour. Res. 2017 (53), 10374–10394. https://doi.org/10.3390/rs12030384.

Tauro, F., Tosi, F., Mattoccia, S., Toth, E., Piscopia, R., Grimaldi, S., 2020. Optical tracking velocimetry (OTV): leveraging optical flow and trajectory-based filtering for surface streamflow observations. Remote Sens. 10 (2010), 2018. https://doi.org/10.3390/rs10122010.

Thielicke, W., Stamhuis, E.J., 2014. PIVlab – towards user-friendly, affordable and accurate digital particle image velocimetry in MATLAB. J. Open Res. Software. https://doi.org/10.5334/jors.bl.

Tosi, F., Rocca, M., Aleotti, F., Poggi, M., Mattoccia, S., Tauro, F., Toth, E., Grimaldi, S., 2020. Enabling image-based streamflow monitoring at the edge. Remote Sens. 2020 (12), 2047.